

A Local Adaptive Threshold Strategy for High Resolution Peripheral Quantitative Computed Tomography of Trabecular Bone

ANDREW J. BURGHARDT, GALATEIA J. KAZAKIA, and SHARMILA MAJUMDAR

Musculoskeletal Quantitative Imaging Research Group, Department of Radiology, University of California, QB3 Building, Suite 203, 1700 4th St, San Francisco, CA 94158, USA

(Received 13 April 2007; accepted 18 June 2007; published online 30 June 2007)

Abstract—High resolution peripheral quantitative computed tomography (HR-pQCT) is a promising method for detailed *in vivo* 3D characterization of the densitometric, geometric, and microstructural features of human bone. Currently, a hybrid densitometric, direct, and plate model-based calculation is used to quantify trabecular microstructure. In the present study, this legacy methodology is compared to direct methods derived from a new local thresholding scheme independent of densitometric and model assumptions.

Human femoral trabecular bone samples were acquired from patients undergoing hip replacement surgery. HR-pQCT (82 μm isotropic voxels) and micro-tomography (16 μm isotropic voxels) images were acquired. HR-pQCT images were segmented and analyzed in three ways: (1) using the hybrid method provided by the manufacturer based on a fixed global threshold, (2) using direct 3D methods based on the fixed global threshold segmentation, and (3) using direct 3D methods based on a novel local threshold scheme. The results were compared against standard direct 3D indices from μCT analysis.

Standard trabecular parameters determined by HR-pQCT correlated strongly to μCT . BV/TV and Tb.Th were significantly underestimated by the hybrid method and significantly overestimated by direct methods based on the global threshold segmentation while the local method yielded optimal intermediate results. The direct-local method also performed favorably for Tb.N ($R^2 = 0.85$ vs. $R^2 = 0.70$ for direct-global method) and Tb.Sp ($R^2 = 0.93$ vs. $R^2 = 0.85$ for the hybrid method and $R^2 = 0.87$ for the direct-global method).

These results indicate that direct methods, with the aid of advanced segmentation techniques, may yield equivalent or improved accuracy for quantification of trabecular bone microstructure without relying on densitometric or model assumptions.

Keywords—High resolution peripheral quantitative computed tomography, Micro-tomography, Trabecular bone, Threshold, Image processing.

Address correspondence to Andrew J. Burghardt, Musculoskeletal Quantitative Imaging Research Group, Department of Radiology, University of California, QB3 Building, Suite 203, 1700 4th St, San Francisco, CA 94158, USA. Electronic mail: andrew.burghardt@radiology.ucsf.edu

INTRODUCTION

Micro-computed tomography (μCT) has become an important tool for investigating a wide range of aspects related to the biology of bone and other calcified tissues.^{8,19,27} Characterization of the microstructural properties of trabecular bone has received considerable attention as an important aspect of bone quality. Until recently, true 3D assessment of trabecular bone microstructure has been limited to *in vitro* measurements in desktop micro-tomography systems.^{4,6}

High resolution peripheral quantitative computed tomography (HR-pQCT) is a promising non-invasive method for *in vivo* 3D characterization of bone in humans. Similar to traditional quantitative computed tomography (QCT), HR-pQCT provides the ability to quantitatively assess volumetric bone mineral density (vBMD) in a compartmental fashion. Additionally, it permits quantification of the geometric, microstructural, and mechanical features of human cortical and trabecular bone in the appendicular skeleton (distal radius and tibia).^{2,11,18} The potential for longitudinal *in vivo* assessment of bone quality with respect to therapeutic efficacy is of particular interest. The most recent generation of this device is capable of an isotropic nominal resolution of 82 μm . This raises the possibility for direct assessment of trabecular bone volume (BV/TV), dimensions (Tb.N, Tb.Th, and Tb.Sp) as well as non-metric descriptors of bone architecture such as structure model index (SMI), degree of anisotropy (DA), and connectivity density (ConnD) which are derived from standard methods used with traditional micro-tomographic evaluations.⁸

The current clinical analysis protocol for assessing trabecular microstructure is based on a hybrid densitometric, direct, and plate-model calculation adapted from the methods used in a previous generation of this device.¹⁶ In this scenario, bone volume fraction (BV/TV) is derived densitometrically from the apparent trabecular bone density and an assumed compact bone

density of 1200 mg HA/cm^3 . A fixed, global threshold is applied to extract the trabecular structure for direct measurement of trabecular number, while $Tb.Th$ and $Tb.Sp$ are derived using plate-model assumptions.¹⁶ The validity and robustness of such assumptions has not been evaluated with respect to real inter-subject or longitudinal effects. Specifically, the assumption of a fixed density for compact bone may be problematic in the context of longitudinal assessment of bone structure where the matrix mineral density is affected. Anticatabolic agents have been shown to increase matrix mineralization in human iliac crest bone by as much as 11.6%.¹ This would be expected to introduce a systematic bias in the BV/TV measure, and in turn the derived trabecular indices. Furthermore, because the size of a human trabecula from the radius or tibia is approximately equivalent to 1 or 2 voxels ($82 \mu\text{m}$), significant partial volume effects make selection of a global threshold challenging. Matrix mineralization effects, which directly affect the image intensity for bone components, further confound this process. For these reasons, a global, fixed threshold may not be the ideal method for extraction of the trabecular structure.

While the resolution of HR-pQCT is not sufficient to accurately depict trabecular dimensions at the level of individual trabeculae, we hypothesize that mean apparent measures, based on a local probabilistic structure extraction method, can be accurately determined in resolution-limited modalities. The goal of the present study was to develop a local structure extraction method for HR-pQCT that (a) is independent of

mineralization and model assumptions and (b) allows accurate and direct assessment of mean trabecular structure indices. The presented method was evaluated against the standard clinical structure extraction and hybrid analysis methods in cadaveric trabecular bone using $16 \mu\text{m}$ micro-tomography as a gold standard.

MATERIALS AND METHODS

Local Threshold Algorithm

A schematic representation of the threshold algorithm is presented in Fig. 1. The algorithm was adapted, in part, from the method presented by Waarsing *et al.* which was developed for small animal *in vivo* micro-tomography.²⁹ Three orthogonal 3D Sobel operators ($3 \times 3 \times 3$) are applied to the input image to compute the intensity gradient magnitude and direction. A non-maximal suppression (NMS) process is then performed on the gradient map to delineate potential edge voxels from background voxels and interior bone voxels: voxels that are not local maxima (using a $3 \times 3 \times 3$ neighborhood) along the gradient direction are set to zero. Next, a discrete edge map is generated by applying a hysteresis threshold algorithm to the remaining edge candidate voxels (henceforth referred to as the non-maximal suppressed gradient map).³ In the hysteresis approach, voxels with gradient magnitudes above a defined cutoff (T_{high}) are considered true edges. These “strong” edge voxels are then used as seeds to trace the object edge and identify

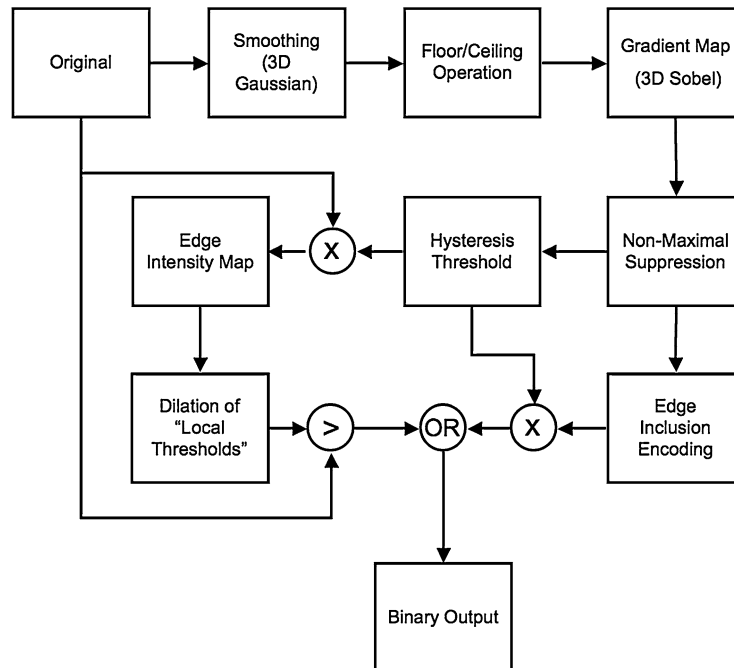


FIGURE 1. Schematic for 3D Sobel-based local threshold algorithm with edge inclusion criteria.

connected “weak” edge components according to a second lower gradient magnitude threshold (T_{low}).

The original grayscale intensities at the newly located edge are then taken as the local threshold criteria for their respective neighborhood. An image-wide local threshold map is determined by an iterative grayscale dilation of these edge intensities. For each dilation iteration border voxels are assigned the Gaussian weighted average of their edge neighbors ($3 \times 3 \times 3$ neighborhood). The resulting image represents a preliminary, voxel-specific local threshold criteria. A simple greater than ($>$) operator is then applied to the attenuation map and local threshold map to delineate object (bone) and background (marrow).

By use of a $>$ operator, the edge voxels are, by definition, excluded from the extracted structure. As an additional step, an edge inclusion criterion was developed to selectively include or exclude edge voxels. Specifically, an edge voxel was included in the final extracted structure based on its similarity to neighbor voxels along the direction of the intensity gradient:

$$B_v = \begin{cases} 1 & \frac{I_v^+ - I_v}{|I_v^- - I_v|} \leq 1 \\ 0 & \frac{I_v^+ - I_v}{|I_v^- - I_v|} > 1 \end{cases}$$

where B_v is the binary inclusion result for the voxel v , I_v is the original intensity at voxel v , I_v^+ is the intensity of the neighbor voxel in the positive gradient direction, and I_v^- is the intensity of the neighbor voxel in the negative gradient direction. Effectively, if the absolute intensity of each edge voxel is closer in magnitude to its bone voxel neighbor along the gradient direction, the edge voxel is determined to be bone. In contrast, if the edge voxel intensity is closer in magnitude to its background voxel neighbor along the gradient direction, the edge voxel is determined to be background. Algorithmically, this was accomplished by encoding B_v (determined at the non-maximal suppression step) into the integer signage for each voxel (which is mathematically disregarded for all subsequent image processing steps). A positive value was used to denote inclusion, while a negative value denoted exclusion. By this process, edge voxels could be categorized as object or background in the final segmentation.

Sample Validation

To evaluate the performance of the threshold scheme presented above, validation experiments using a micro-tomography gold standard were performed in cadaveric bone tissue. Three femoral head specimens were acquired from patients with degenerative joint disease, undergoing total hip replacement surgery. A

total of 11 trabecular bone cores, measuring 8 mm in diameter and approximately 10 mm in length, were extracted from the superior and inferior aspects of the femoral head. Subchondral bone, immediately adjacent to the diseased articular surface, was excluded. The bone marrow was removed using cycled treatment with a mild bio-detergent (Terg-A-Zyme, Alconox Inc) in sonicated water bath. The samples were then embedded in polymethyl methacrylate (PMMA) prior to imaging.

High Resolution Peripheral Quantitative Computed Tomography

All femoral core samples were first imaged in a clinical HR-pQCT system (XtremeCT, Scanco Medical AG, Bassersdorf, Switzerland) using the standard *in vivo* protocol described in previous patient studies.^{2,11} In short, the X-ray source potential was 60 kVp with a current of 900 μ A. A 2D 3072 \times 256 element CCD detector was used to acquire 750 projections at a 100 ms integration time per rotation. The 12.6 mm field of view (FOV) was reconstructed across a 1536 \times 1536 matrix, yielding 82 μ m voxels. The full length of each core was covered by the automatic acquisition of two adjacent image stacks, spanning 9.05 mm each. Total scan time was 5.6 min. The reconstructed linear attenuation values were calibrated to hydroxyapatite (HA) mineral densities based on a separate measurement of a phantom comprised of cylinders with various HA concentrations.

Micro-tomography

To serve as a reference for trabecular structure indices, high-resolution micro-tomography (μ CT) images were acquired for each sample using a desktop *in vitro* μ CT system (μ CT-40, Scanco Medical AG, Bassersdorf, Switzerland). This device consists of a micro-focus X-ray source that produces a narrow angle cone beam incident upon a 2048 \times 64 element CCD detector. A previous generation of this scanner has been described in detail.²⁵ Using a 70 kVp source potential and 114 mA current, 500 projection images were collected spanning 180° degrees with each projection sampled for 250 ms. The projections were then reconstructed across a 1024 \times 1024 matrix spanning a 16.4 mm FOV and resulting in an isotropic nominal resolution of 16 μ m. Total scan time was approximately 6 h.

Hybrid Analysis

HR-pQCT images were initially evaluated using the standard clinical evaluation protocol, adapted from

methods developed for a previous pQCT device.^{14,16} In this scenario, BV/TV is derived from the volumetric BMD of the trabecular ROI ($vBMD_{\text{trab}}$) and making the assumption that compact bone has a matrix mineral density of 1200 mg HA/cm³ while the marrow background is equivalent to 0 mg HA/cm³. Extraction of the trabecular structure is performed as follows: A Laplace–Hamming filter—which effectively smoothes the image and enhances edges—is applied to the original grayscale data. Second, the smoothed image is normalized to a fixed intensity value. Finally, a fixed global threshold (40% of the positive integer space) is applied to discretize the bone and background phases.¹⁷ From the binary image, Tb.N* is measured using direct 3D methods.⁹ Based on the densitometric BV/TV and direct Tb.N*, Tb.Th, and Tb.Sp are derived using traditional plate model assumptions.²¹ This method will subsequently be referred to as the “hybrid” method.

Direct Analysis

All image datasets (HR-pQCT and μ CT) were evaluated using direct 3D methods. Direct analysis for HR-pQCT images was performed based on both global (taken as the structure extraction from the hybrid method) and local threshold methods. The segmentation from the hybrid analysis was used for direct-global calculations. Prior to application of the local threshold routine, the grayscale values were smoothed with a Gaussian filter ($\sigma = 0.5$, kernel = 3) and then truncated to a maximum intensity equivalent to 950 mg HA/cm³. Local threshold parameters T_{high} and T_{low} were determined automatically for each sample based on the histogram of the NMS gradient magnitude image. A simple Gaussian curve was fit to the high intensity peak (representing the true edges) in the bimodal histogram. T_{high} was defined as the mean of the Gaussian fit, while T_{low} was defined as 1.5 standard deviations below the mean. A fixed global threshold (visually selected as 25% of the positive integer space) was used to segment the bone phase for all μ CT images.

Based on these segmentations, BV/TV was determined by simple voxel counting of the bone and background phases. Mean trabecular dimensions (Tb.Th*, Tb.N*, and Tb.Sp*) and the corresponding standard deviations parameters (Tb.Th.SD*, Tb.(1/N).SD*, and Tb.Sp.SD*) were calculated directly using a model-independent sphere filling technique.⁹ Degree of anisotropy (DA) was calculated as the ratio of major and minor principal components of the MIL ellipsoid.⁷ Connectivity density (ConnD) was calculated based on the Euler number.²⁰ Finally, structure model index (SMI), a measure of surface convexity, was calculated from a triangulated surface representation of the 3D

binary data.¹⁰ Results based on this method will subsequently be referred to as the “direct-global” and “direct-local” methods for HR-pQCT and simply as the “direct” method for μ CT.

Statistics

Regression analysis was performed to compare all HR-pQCT methods against indices measured by direct methods based on the μ CT images. The R^2 values as well as the linear equations relating HR-pQCT derived indices to the reference μ CT indices were calculated. Additionally, significant differences between HR-pQCT and μ CT measures were determined by a paired t -test.

RESULTS

Independent, direct measures of trabecular bone structure based on the presented local threshold algorithm generally performed equivalent to, or better than, hybrid methods that rely on densitometric and structure model assumptions. The intermediate steps in the local threshold algorithm are presented in Fig. 2 for a representative femoral core sample. The image output for the global and local threshold methods are shown in Fig. 3, including the grayscale μ CT, grayscale HR-pQCT, and binarized HR-pQCT images segmented by global and local threshold schemes. In general, the local threshold method visually appeared to better represent the trabecular thickness compared to the global extraction, which appeared to overestimate thickness. At the same time the local threshold result appeared to mostly retain connectedness of the trabecular elements.

The absolute mean and standard deviation values for all parameters calculated by direct, hybrid, direct-global, and direct-local methods is presented in Table 1. HR-pQCT results that were significantly different ($p < 0.05$) from the corresponding μ CT derived result are denoted (*). The regression analysis for the standard metric parameters is presented in Fig. 4. All standard HR-pQCT derived indices were found to perform well against the μ CT gold standard with $R^2 > 0.85$ ($p < 0.0001$) with the exception of Tb.N* calculated from the direct-global segmentation which was moderately well correlated ($R^2 = 0.70$, $p < 0.01$). The distribution parameters (Tb.Th.SD*, Tb.(1/N).SD*, and Tb.Sp.SD*) performed less reliably ($R^2 = 0.47$ – 0.78) while non-metric indices had mixed results. Connectivity density was found to perform particularly poorly (R^2 0.43 for direct-global and $R^2 = 0.48$ for direct-local, $p < 0.05$ for both) while SMI and DA performed well for global and local

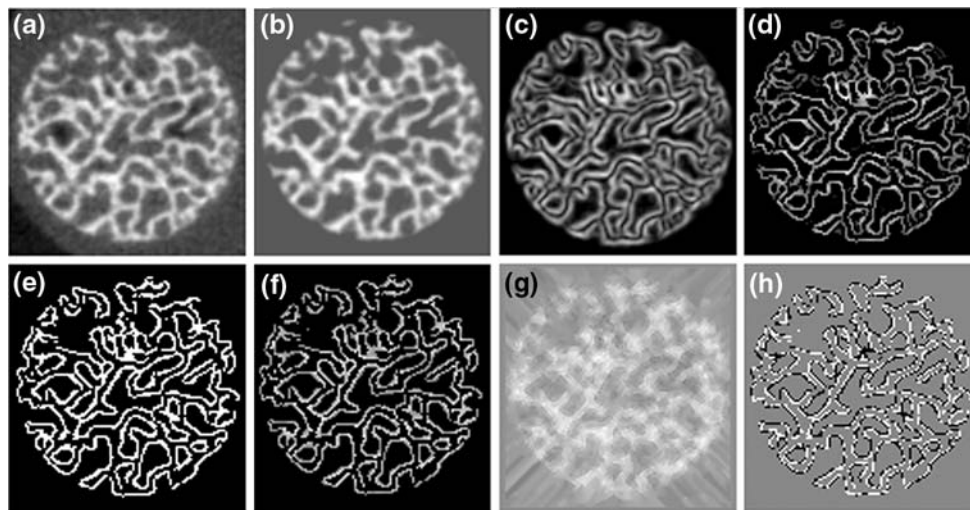


FIGURE 2. Representative images for steps in the local threshold process. (a) Original attenuation map, (b) ceiling step, (c) Sobel gradient magnitude, (d) non-maximal suppression, (e) binary edge map, (f) edge attenuation map, (g) local threshold map, and (h) edge inclusion map (black = excluded edge pixels, white = included edge pixels).

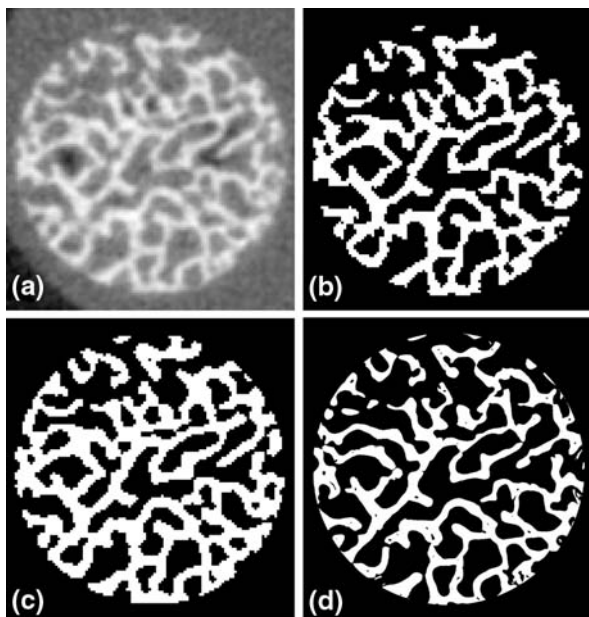


FIGURE 3. Representative 2D image for: (a) original HR-pQCT attenuation map, (b) HR-pQCT segmented with local threshold method, (c) HR-pQCT segmented by global threshold method, and (d) binary μ CT image of corresponding slice.

methods ($R^2 = 0.78$, 0.90 and $R^2 = 0.92$, 0.86 , respectively, with $p < 0.001$ for direct-global SMI and $p < 0.0001$ for the rest). The distribution and non-metric parameters are presented in Fig. 5.

DISCUSSION

In this study an improved method for structure extraction has been developed and applied to images of

trabecular bone acquired with a new *in vivo* micro-tomography system designed to image distal extremities in humans. Using high-resolution micro-tomography as a gold standard, this local, adaptive method was evaluated against the current method that relies on a global threshold, density assumptions, and derived indices for bone volume and trabecular dimensions. As a tool targeted for longitudinal assessment of bone microstructure, HR-pQCT-based analyses should ideally be independent of bone material properties that may be affected under experimental conditions such as therapeutic intervention and pathological progression. In the proposed method, a gradient-based edge detection technique is used to extract the trabecular structure irrespective of the absolute image intensity values, and used to directly quantify bone volume, structure metrics, and non-metric indices.

Trabecular bone cores from the proximal femur were selected for this study because they were conveniently available from routine hip replacement procedures performed onsite. While this is not an anatomic site used for clinical HR-pQCT examinations, the range of values for most parameters overlapped with typical values for the distal radius and distal tibia. Critically, the mean Tb.Th* for the femur samples, as determined by μ CT, was approximately the same as distal tibia and radius values reported in the literature.^{12,18} While the correlations for BV/TV were strong for all analysis methods, densitometrically derived BV/TV—based on an assumed compact bone density of 1200 mg HA/cm^3 —resulted in a significant underestimation relative to the μ CT gold standard (slope = 1.12). On the other hand, direct calculation of bone volume based on the global threshold segmentation

TABLE 1. Mean and standard deviation of trabecular indices.

Parameter	μ CT (direct)	HR-pQCT (hybrid)	HR-pQCT (direct-global)	HR-pQCT (direct-local)
BV/TV	0.26 ± 0.13	0.26 ± 0.12	0.39 ± 0.15*	0.32 ± 0.14*
Tb.N	1.70 ± 0.49	1.78 ± 0.32*	1.78 ± 0.32*	1.87 ± 0.46*
Tb.Th	0.18 ± 0.05	0.14 ± 0.05*	0.25 ± 0.05	0.20 ± 0.04*
Tb.Sp	0.60 ± 0.15	0.44 ± 0.15*	0.50 ± 0.15*	0.54 ± 0.16*
Tb.(1/N).SD	0.24 ± 0.04	0.21 ± 0.06	0.21 ± 0.06	0.24 ± 0.06
Tb.Th.SD	0.07 ± 0.01	–	0.09 ± 0.02*	0.06 ± 0.02*
Tb.Sp.SD	0.22 ± 0.04	–	0.21 ± 0.06	0.23 ± 0.06
ConnD	9.11 ± 5.44	–	3.06 ± 0.95*	4.23 ± 1.85*
SMI	0.64 ± 1.18	–	0.23 ± 2.36	0.48 ± 1.52
DA	1.65 ± 0.27	–	1.57 ± 0.30*	1.50 ± 0.25*

*Indicates HR-pQCT results that are significantly different from the direct μ CT values ($p < 0.05$).

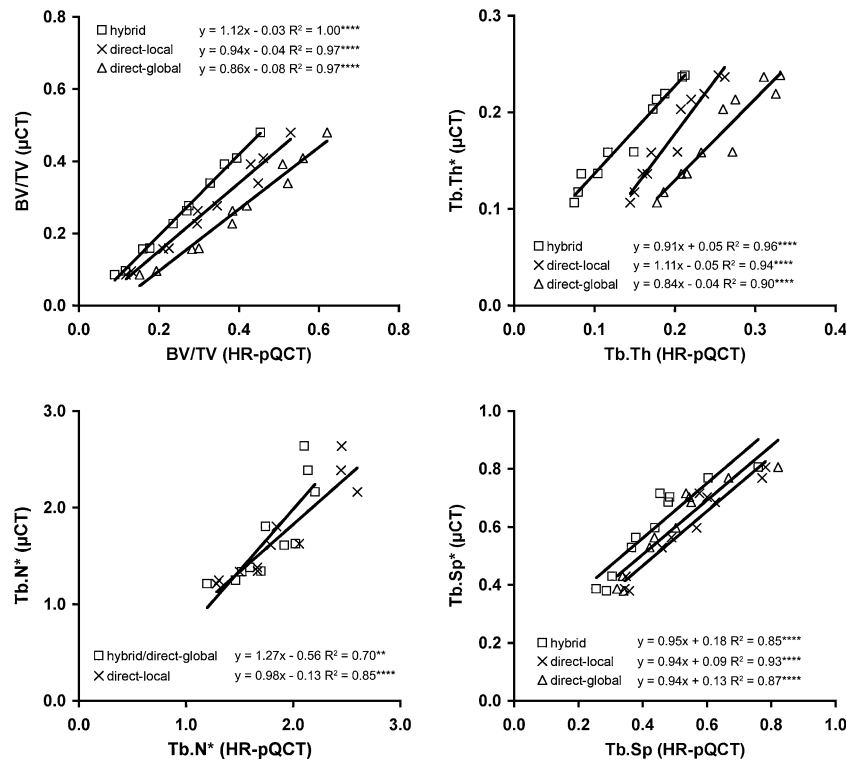


FIGURE 4. Plots for hybrid, direct-global, and direct-local HR-pQCT calculations compared against direct μ CT methods for BV/TV, Tb.Th, Tb.N, and Tb.Sp. Regression analysis R^2 , slopes, and intercepts are given for each method and parameter. All correlations were statistically significant ($p < 0.01$, **** $p < 0.0001$).**

significantly overestimated BV/TV. The direct-local method yielded the most accurate absolute values, which were modestly overestimated. Similarly, Tb.Th was significantly underestimated when derived in the hybrid analysis scheme, and significantly overestimated when measured directly based on a global threshold. The direct-local method yielded optimal intermediate results that were somewhat overestimated. Previous bone morphometry studies have consistently found that Tb.N is most accurately determined using limited resolution modalities.^{13,16,18} Surprisingly, Tb.N* performed least well in this study

among the standard trabecular metrics ($R^2 = 0.70$ for global, $R^2 = 0.85$ for local). Finally, the direct-local method yielded the strongest correlation to, and most accurately measured (as per the regression slope and intercept) μ CT derived Tb.Sp.

The standard deviation trabecular dimension parameters, which quantify the degree of structural heterogeneity and have previously been shown to be potential predictors of fracture risk,¹⁵ were moderately well correlated to direct μ CT values, though not as strongly as previously reported in a study using high-resolution MRI.¹³ The slope and intercept of the

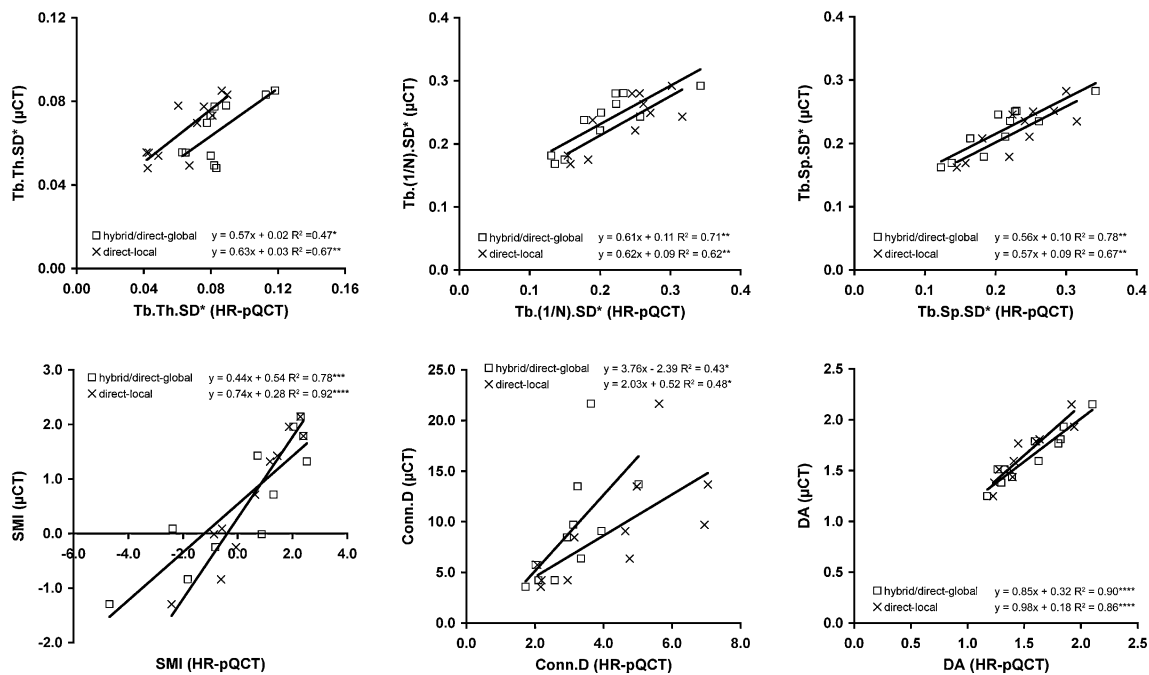


FIGURE 5. Plots for hybrid, direct-global, and direct-local HR-pQCT calculations compared against direct μ CT methods for Tb.Th.SD, Tb.(1/N).SD, Tb.Sp.SD, SMI, ConnD, and DA. Regression analysis R^2 , slopes, and intercepts are given for each method and parameter. All correlations were statistically significant ($^*p < 0.05$, $^{**}p < 0.01$, $^{***}p < 0.001$, $^{****}p < 0.0001$).

regression equations were comparable between methods; the intercepts were relatively large and the slopes were somewhat low. The coefficient of determination was somewhat lower for Tb.Sp.SD* and Tb.(1/N).SD* using the direct-local analysis, while Tb.Th.SD* was substantially higher ($R^2 = 0.67$ vs. $R^2 = 0.47$).

Structure model index (SMI) performed moderately well, particularly when using the local threshold segmentation ($R^2 = 0.78$ for direct-global method, $R^2 = 0.92$ for direct-local method). In contrast, MacNeil and Boyd found a much lower correlation for SMI in the human distal radius.¹⁸ This is likely due to the dramatic difference in structure types between these sites. While the ultra-distal radius is predominantly comprised of rod-like elements, trabecular bone from the proximal femur can span a much wider range of structure types, as seen here and elsewhere.⁸ The tibia, like the proximal femur, tends toward a more mixed and plate-like architecture,^{5,12} and therefore may be better represented by these results. The negative SMI values are characteristic of higher-density bone architectures and indicate a prevalence of concave surfaces (fenestrations or tubular pore spaces). ConnD performed poorly for both methods, and in general was underestimated by a factor of 2 for the direct-local method and 3 for the direct-global method. This observation is also considerably different from what MacNeil and Boyd found in the distal radius¹⁸ where samples with a much lower ConnD (2 ± 1)

correlated very strongly to μ CT derived values ($R^2 = 0.91$). DA performed equally well using the global and local threshold methods ($R^2 = 0.90$ vs. $R^2 = 0.86$ respectively). Collectively, these results and the related literature indicate that the accuracy of HR-pQCT analysis methods exhibit a strong site dependence. As a result, this study may provide a better indication of how these methods perform with respect to clinical evaluation of the distal tibia more so than the distal radius. Further evaluation of these site dependent effects should be considered in the future.

Since human trabecular bone from the distal radius and tibia has a mean thickness approximately equivalent to 2 voxels at HR-pQCT resolutions ($82 \mu\text{m}$), partial volume components comprise a significant fraction of the total bone volume. As a result, segmentation of the trabecular microstructure, for the purposes of quantification, is a challenging process. The manufacturer's method, which has been validated in cross-sectional normal specimen studies,^{16,18} relies in part on plate model assumptions and an assumed compact tissue density. In this hybrid analysis approach, only Tb.N* is measured directly. For this reason, the segmentation is optimized to preserve all trabeculae, while not artificially closing small pore spaces or including noise voxels as trabeculae. Representation of the trabecular thickness and separation is not important in this scenario, therefore a relatively low global threshold is used which assigns a substantial

portion of partial volume voxels to the bone phase rather than marrow. Since direct assessment of Tb.N* does not rely on an accurate depiction of the trabecular thickness, this is sufficient, and instead Tb.Th and Tb.Sp are derived from Tb.N* and the densitometric BV/TV using plate model relations.

It is not clear how changes in matrix level mineral density could impact results based on the hybrid structure analysis. Using microradiography, Boivin and colleagues observed a difference of 11.4% in the tissue-level mineral density of iliac crest biopsies in alendronate treated patients (3 years) compared to matched placebo controls.¹ While this would clearly be expected to bias derived BV/TV measures, it could also impact the Tb.N* which relies on a fixed global threshold. These observations provided the motivation for developing local, adaptive segmentation methods that would permit direct calculation of trabecular dimensions and volume, independent of densitometric assumptions and spatial or temporal variability in trabecular mineralization.

A novel aspect of the algorithm presented here is an inclusion criterion for edge pixels. Again, due to resolution limitations for *in vivo* HR-pQCT, the fraction of bone pixels that also represent the bone-marrow edge is substantial compared to *ex vivo* micro-tomography where an average trabecula might span 10 pixels in diameter. The criterion, which considers the similarity of a given edge pixel to its neighbor pixels along the direction of the intensity gradient, effectively tests the probability that the pixel is primarily comprised of bone or marrow. Compared to complete exclusion or inclusion of edge pixels, using the proposed inclusion criterion yielded substantially improved coefficients of determination and regression equations (data not shown).

Segmentation of the bone-marrow edge by hysteresis thresholding of the NMS gradient map requires two input parameters: (1) a high threshold to identify all strong edge components, and (2) a lower threshold to capture the contiguous weak edge components. For the purposes of this study these parameters were calculated automatically from the NMS gradient histogram, which was approximately bimodal. The large peak at the lower end of the gradient spectrum represents texture in the image background while the smaller peak for higher gradient voxels represents the true bone-marrow edge. The latter was fit with a Gaussian function from which the mean and standard deviation were used to define the hysteresis thresholds. While this method was sufficient here to demonstrate the utility of the presented local threshold algorithm, a full parameter study would be necessary for optimal *in vivo* performance where patient motion, increased beam hardening, lower SNR, and dose limitations limit contrast and resolution.

An additional advantage to the presented local, adaptive approach is that cortical and trabecular compartments can be accurately extracted in a single threshold step. The traditional approach accomplishes this in two steps. The cortex is segmented by applying a strong Gaussian blurring filter ($\sigma = 1.5$, kernel = 7) to wash out the trabecular structure, followed by a fixed threshold. This again assumes a fixed compact bone density. Furthermore, it often eliminates thin cortical components in the ultra-distal radius and macro-porosity. As described earlier, the trabecular bone segmentation relies on a different fixed threshold. The independent segmentation of the trabecular bone and cortex may lead to significant discontinuities between these compartments which in turn would be expected to have a dramatic impact on apparent strength measures determined by micro-finite element analysis.^{18,22,23,28} Alternatively, models constructed using the global threshold of the hybrid analysis (which is optimized for extraction of the trabecular bone compartment) would be expected to overestimate cortical mass. This scenario would also affect apparent mechanical properties²⁴ and specifically misrepresent load sharing between cortical and trabecular compartments.²⁶ While a more detailed evaluation of these variables, as they relate to the accurate construction of mechanical models, is necessary, the local adaptive segmentation method presented here may provide a useful approach to the segmentation problem for HR-pQCT-based finite element analysis.

In summary, a new local, adaptive threshold method was developed that performed equivalent, and in some cases superior to a simple global threshold segmentation applied to HR-pQCT images of trabecular bone. Analyses independent of densitometric and model assumptions would be important for unbiased longitudinal assessment of skeletal effects due to therapeutic intervention or pathological progression. As a more complicated image-processing scheme, additional variables come into play which require more extensive validation for application to true *in vivo* scenarios. Furthermore, such optimizations should be independently evaluated for microstructural and mechanical analyses. Finally, this method is potentially applicable to other modalities for high-resolution imaging of porous materials, including micro-tomography and magnetic resonance imaging (MRI) where global thresholds are still the common method for segmentation.

ACKNOWLEDGMENTS

The authors would like to acknowledge funding support from NIH RO1 AG17762 (SM). Furthermore,

they would like to thank Dr. Andres Laib and Scanco Medical AG for providing software development consultation and for providing an API for IPL (Image Processing Language, Scanco Medical AG, Bassersdorf, Switzerland). They would also like to thank Dr. Michael Ries of the UCSF Department of Orthopaedic Surgery for providing the tissue used in this study.

REFERENCES

- ¹Boivin, G. Y., P. M. Chavassieux, A. C. Santora, J. Yates, and P. J. Meunier. Alendronate increases bone strength by increasing the mean degree of mineralization of bone tissue in osteoporotic women. *Bone* 27(5):687–694, 2000.
- ²Boutroy, S., M. L. Bouxsein, F. Munoz, and P. D. Delmas. *In vivo* assessment of trabecular bone microarchitecture by high-resolution peripheral quantitative computed tomography. *J. Clin. Endocrinol. Metab.* 90(12):6508–6515, 2005.
- ³Canny, J. A computational approach to edge detection. *IEEE Trans. Pattern Anal. Mach. Intell.* 8:679–698, 1986.
- ⁴David, V., N. Laroche, B. Boudignon, M. H. Lafage-Proust, C. Alexandre, P. Ruegsegger, and L. Vico. Non-invasive *in vivo* monitoring of bone architecture alterations in hindlimb-unloaded female rats using novel three-dimensional microcomputed tomography. *J. Bone Miner. Res.* 18(9):1622–1631, 2003.
- ⁵Ding, M., and I. Hvid. Quantification of age-related changes in the structure model type and trabecular thickness of human tibial cancellous bone. *Bone* 26(3):291–295, 2000.
- ⁶Gasser, J. A., P. Ingold, K. Grosios, A. Laib, S. Hammerle, and B. Koller. Noninvasive monitoring of changes in structural cancellous bone parameters with a novel prototype micro-CT. *J. Bone Miner. Metab.* 23(Suppl):90–96, 2005.
- ⁷Harrigan, T. P., and R. W. Mann. Characterization of microstructural anisotropy in orthotropic materials using a second rank tensor. *J. Mater. Sci.* 19:761–767, 1984.
- ⁸Hildebrand, T., A. Laib, R. Muller, J. Dequeker, and P. Ruegsegger. Direct three-dimensional morphometric analysis of human cancellous bone: microstructural data from spine, femur, iliac crest, and calcaneus. *J. Bone Miner. Res.* 14(7):1167–1174, 1999.
- ⁹Hildebrand, T., and P. Ruegsegger. A new method for the model-independent assessment of thickness in three-dimensional images. *J. Microsc.* 185:67–75, 1997.
- ¹⁰Hildebrand, T., and P. Ruegsegger. Quantification of bone microarchitecture with the structure model index. *Comput. Methods Biomech. Biomed. Eng.* 1(1):15–23, 1997.
- ¹¹Khosla, S., B. L. Riggs, E. J. Atkinson, A. L. Oberg, L. J. McDaniel, M. Holets, J. M. Peterson, and L. J. Melton III. Effects of sex and age on bone microstructure at the ultradistal radius: a population-based noninvasive *in vivo* assessment. *J. Bone Miner. Res.* 21(1):124–131, 2006.
- ¹²Lai, Y. M., L. Qin, V. W. Hung, W. Y. Choy, S. T. Chan, L. W. Chan, and K. M. Chan. Trabecular bone status in ultradistal tibia under habitual gait loading: a pQCT study in postmenopausal women. *J. Clin. Densitom.* 9(2):175–183, 2006.
- ¹³Laib, A., O. Beuf, A. Issever, D. C. Newitt, and S. Majumdar. Direct measures of trabecular bone architecture from MR images. *Adv. Exp. Med. Biol.* 496:37–46, 2001.
- ¹⁴Laib, A., H. J. Hauselmann, and P. Ruegsegger. *In vivo* high resolution 3D-QCT of the human forearm. *Technol. Health Care* 6(5–6):329–337, 1998.
- ¹⁵Laib, A., D. C. Newitt, Y. Lu, and S. Majumdar. New model-independent measures of trabecular bone structure applied to *in vivo* high-resolution MR images. *Osteoporos. Int.* 13(2):130–136, 2002.
- ¹⁶Laib, A., and P. Ruegsegger. Calibration of trabecular bone structure measurements of *in vivo* three-dimensional peripheral quantitative computed tomography with 28-microm-resolution microcomputed tomography. *Bone* 24(1):35–39, 1999.
- ¹⁷Laib, A., and P. Ruegsegger. Comparison of structure extraction methods for *in vivo* trabecular bone measurements. *Comput. Med. Imaging Graph.* 23(2):69–74, 1999.
- ¹⁸Macneil, J. A. and S. K. Boyd. Accuracy of high-resolution peripheral quantitative computed tomography for measurement of bone quality. *Med Eng Phys.* Jan 15, 2007.
- ¹⁹Muller, R., and P. Ruegsegger. Micro-tomographic imaging for the nondestructive evaluation of trabecular bone architecture. *Stud. Health Technol. Inform.* 40:61–79, 1997.
- ²⁰Odgaard, A., and H. J. Gundersen. Quantification of connectivity in cancellous bone, with special emphasis on 3-D reconstructions. *Bone* 14(2):173–182, 1993.
- ²¹Parfitt, A. M., M. K. Drezner, F. H. Glorieux, J. A. Kanis, H. Malluche, P. J. Meunier, S. M. Ott, and R. R. Recker. Bone histomorphometry: standardization of nomenclature, symbols, and units. Report of the ASBMR Histomorphometry Nomenclature Committee. *J. Bone Miner. Res.* 2(6):595–610, 1987.
- ²²Pistoia, W., B. van Rietbergen, A. Laib, and P. Ruegsegger. High-resolution three-dimensional-pQCT images can be an adequate basis for in-vivo microFE analysis of bone. *J. Biomech. Eng.* 123(2):176–183, 2001.
- ²³Pistoia, W., B. van Rietbergen, E. M. Lochmuller, C. A. Lill, F. Eckstein, and P. Ruegsegger. Estimation of distal radius failure load with micro-finite element analysis models based on three-dimensional peripheral quantitative computed tomography images. *Bone* 30(6):842–848, 2002.
- ²⁴Pistoia, W., B. van Rietbergen, and P. Ruegsegger. Mechanical consequences of different scenarios for simulated bone atrophy and recovery in the distal radius. *Bone* 33(6):937–945, 2003.
- ²⁵Ruegsegger, P., B. Koller, and R. Muller. A microtomographic system for the nondestructive evaluation of bone architecture. *Calcif. Tissue Int.* 58(1):24–29, 1996.
- ²⁶Ulrich, D., B. van Rietbergen, A. Laib, and P. Ruegsegger. Load transfer analysis of the distal radius from in-vivo high-resolution CT-imaging. *J. Biomech.* 32(8):821–828, 1999.
- ²⁷Ulrich, D., B. van Rietbergen, A. Laib, and P. Ruegsegger. The ability of three-dimensional structural indices to reflect mechanical aspects of trabecular bone. *Bone* 25(1):55–60, 1999.
- ²⁸van Rietbergen, B., S. Majumdar, W. Pistoia, D. C. Newitt, M. Kothari, A. Laib, and P. Ruegsegger. Assessment of cancellous bone mechanical properties from micro-FE models based on micro-CT, pQCT and MR images. *Technol. Health Care.* 6(5–6):413–420, 1998.
- ²⁹Waarsing, J. H., J. S. Day, and H. Weinans. An improved segmentation method for *in vivo* microCT imaging. *J. Bone Miner. Res.* 19(10):1640–1650, 2004.